 doi:10.20944/preprints202208.0340.v1

Altered microRNA transcriptome in cultured human airway cells upon infection with SARS-CoV-2

Idrissa Diallo[1], Rajesh Abraham Jacob[2], Elodie Vion[1], Robert A. Kozak[3], Karen Mossman[2] and Patrick Provost[1,*]

[1] CHU de Québec-Université Laval Research Center/CHUL Pavilion, Department of Microbiology, Infectious Diseases and Immunology, Faculty of Medicine, Université Laval, Quebec City, QC, G1V 0A6, Canada.
[2] McMaster Immunology Research Centre, M.G. DeGroote Institute for Infectious Disease Research, Department of Medicine, McMaster University, Hamilton, ON L8S 4K1, Canada.
[3] Division of Microbiology, Department of Laboratory Medicine & Molecular Diagnostics, Sunnybrook Health Sciences Centre, Toronto, ON M4N 3M5, Canada.
The first two authors contributed equally to this work.
* Correspondence: Co-corresponding author: Dr. Patrick Provost; Phone: 1 418 525 4444 (ext. 48842); E-mail: patrick.provost@crchudequebec.ulaval.ca

Abstract: Numerous proteomic and transcriptomic studies have been carried out to better understand the current multi-variant SARS-CoV-2 virus mechanisms of action and effects. However, they are mostly centered on mRNAs and proteins. The effect of the virus on human post-transcriptional regulatory agents such as microRNAs (miRNAs) involved in the regulation of 60% of human gene activity remains poorly explored. Similar to what we have previously done with other viruses such as Ebola and HIV, in this study we investigated the miRNA profile of lung epithelial cells following infection with SARS-CoV-2. At the 24 and 72 hours post-infection, SARS-CoV-2 did not drastically alter the miRNome. About 90% of the miRNAs remained non-differentially expressed. The results revealed that miR-1246, miR-1290 and miR-4728-5p were the most upregulated over time. miR-196b-5p and miR-196a-5p were the most downregulated at 24 h while at 72 h, miR-3924, miR-30e-5p and miR-145-3p showed the highest level of downregulation. In the top significantly enriched KEGG pathways of genes targeted by differentially expressed miRNAs we found, among others, MAPK, RAS, P13K-Akt and renin secretion signaling pathways. By RT-qPCR, we also showed that SARS-CoV-2 may regulate several predicted host mRNA targets involved in the entry of the virus into host cells (ACE2, TMPRSS2, ADAM17 and FURIN), in renin–angiotensin system (RAS) (Renin, Angiotensinogen, ACE), innate immune response (IL-6, IFN1β, CXCL10, SOCS4) and fundamental cellular processes (AKT, NOTCH, WNT). Finally, we demonstrated by dual luciferase assay a direct interaction between miR-1246 and ACE-2 mRNA. This study highlights the modulatory role of miRNAs in the pathogenesis of SARS-CoV-2.

Keywords: SARS-CoV-2; RNA-Seq; miRNA; miR-1246; ACE2; Calu-3

Introduction

Two years after the outbreak of the coronavirus disease 19 (COVID-19) pandemic, the disease remains a major public health concern with millions of deaths and hospitalizations reported [1]. Its infectious agent, Severe Acute Respiratory Syndrome CoronaVirus 2 (SARS-CoV-2), a new betacoronavirus of the coronaviridae family [2], has not revealed all secrets despite the global efforts of the scientific community and political leaders.

Although the availability of vaccines and drugs which helped reduce deaths and hospitalizations [3] have given new hope in the fight against the pandemic, we are still threatened by the emergence of concerning variants. It is

 doi:10.20944/preprints202208.0340.v1

therefore important to deepen our understanding of SARS-COV-2, to better characterize the molecular mechanisms that underlie its zoonotic transfer, replication, persistence, transmission, and lethality [4].

SARS-CoV-2 is a positive-sense single-stranded RNA virus and is composed of several accessory proteins and four structural proteins including envelope (E), membrane (M), nucleocapsid (N) and spike (S) [5]. The latter, spike (S), mediates the entry of the virus into host cells by interacting with angiotensin-converting enzyme 2 (ACE2) and other proteases such as transmembrane serine protease 2 (TMPRSS2), ADAM metallopeptidase domain 17 (ADAM17) and Furin [6–8]. The virus leads to an acute respiratory distress syndrome, systemic hyper-inflammation (leading to "cytokine storm") and multiple organ failure [9].

In addition to being poorly understood, the molecular mechanisms behind the immunopathogenesis of COVID19 is often investigated only from the perspective of protein macromolecules [10]. The role of non-coding RNAs in COVID19, in particular microRNAs (miRNAs), is not fully comprehended. However, it is now acknowledged that miRNAs influence more than 60% of a given host transcriptome [11].

miRNAs are 19 to 24-nucleotide (nt) RNAs which induce posttranscriptional repression of their mRNA targets (for review, see [12]) and have been viewed as a possible approach to prevent SARS-CoV-2 replication [13]. Nevertheless, miRNAs may, under certain conditions, be the Achilles heel of the immune defense that SARS-CoV-2 would exploit [14]. This functional duality illustrates the critical role of miRNAs in viral infections [15] and their potential utility as informative biomarkers for disease diagnosis and prognosis [16,17].

In the ongoing pandemic, timely reports (about thirty quality publications released before the end of 2020) provided evidence on the impact of miRNAs on SARS-CoV-2 infection and COVID-19 [18]. Subsequently, further studies performed comprehensive miRNA profiling in various tissues [19–21]. However, in the context of COVID-19, few studies have been conducted to explore the global profile of miRNAs (miRNome) by deep sequencing technologies, especially in the lung, the primary organ targeted by the virus [22–24].

In the current study, we profiled the miRNome at three time points (24 h, 48 h and 72 h) following SARS-CoV-2 infection of lung epithelial cells by RNA-Sequencing (RNA-Seq). Our results reveal that 90% of the miRNAs were non-differentially expressed and that only a limited pool of miRNAs (69 miRNAs at 24 h and 25 miRNAs at 72 h) was specifically modulated by the virus. In the top significantly enriched KEGG pathways of genes targeted by differentially expressed miRNAs, we found, among others, MAPK, RAS, P13K-Akt and renin secretion signaling pathways. Using RT-qPCR, we also showed that SARS-CoV-2 may regulate several predicted host mRNA targets involved in the entry of the virus into the host cells (ACE2, TMPRSS2, ADAM17 and Furin), renin–angiotensin–aldosterone system (RAAS) (Renin, Angiotensinogen, ACE), innate immune response (IL-6, IFN1β, CXCL10, SOCS4) and fundamental cellular processes (AKT, NOTCH, WNT). RNA-Seq data highlighted a significant upregulation of miR-1246 (confirmed by RT-qPCR), which was competent in a dual luciferase assay to directly modulate ACE2 via its 3'UTR.

 doi:10.20944/preprints202208.0340.v1

Materials and Methods

Cell culture conditions

Calu-3. The lung adenocarcinoma-derived Calu-3 epithelial cell line (ATCC® HTB-55™, Burlington, Ontario, Canada), was cultured in Minimum Essential Medium (α-MEM) supplemented with 10% fetal bovine serum, 1 mM L-glutamine, 100 units/mL penicillin, and 100 µg/mL streptomycin, incubated at 37 °C in a humidified atmosphere containing 5% CO_2 and passaged every 2 days.

VeroE6: Vero E6 cells (ATCC, CRL-1586™) were cultured in Dulbecco's Modified Eagle's media (DMEM) supplemented with 10% fetal bovine serum, 1x L-glutamine, 100 units/mL penicillin, and 100 µg/mL streptomycin, incubated at 37 °C in a humidified atmosphere containing 5% CO_2.

SARS-CoV-2 viruses. The clinical isolates of SARS-CoV-2 (SARS-CoV-2/SB3) were purified from COVID-19 infected patients in Toronto, Canada and characterized previously [25]. The viral titers were determined using a $TCID_{50}$ assay using Vero E6 cells. Experiments with SARS-CoV-2 were conducted with all precautions in a Biosafety Level 3 laboratory facility. All procedures were approved by the institutional biosafety committees at McMaster University. Calu-3 cells were infected with the SB3 isolate at an MOI of 1.0 in (biological) triplicate with SARS-CoV-2 as previously described [25]. Samples were collected at 24 h, 48 h, and 72 h post transfection. Mock infections were included for each time point. The effectiveness of the infection was validated by qPCR and Western blot through the assessment of viral nucleocapsid mRNA and protein levels respectively.

Protein Extractions and Western Blot

Cultured Calu-3 cells were lysed in RIPA buffer containing complete™ EDTA-free protease inhibitor cocktails (Sigma-Aldrich, Cat #R0278, QC, Canada) and PhosSTOP™ phosphatase inhibitor (Thermo Scientific, Cat # 78446, QC, Canada). Purified proteins were mixed with SDS-loading buffer, denatured (10 min at 95°C) and separated by SDS-PAGE (10% acrylamide gel) after which they were transferred to a PVDF membrane. Membranes were probed with the following primary antibodies: anti-tubulin (1/10000; SCBT, Cat. #sc-5274, TX, USA,) and anti-SARS-CoV-2 nucleocapsid (1/2500; Invitrogen, Cat. # MA5-29981, Invitrogen, ON, Canada) at 4°C overnight, followed by incubation with the corresponding secondary antibodies. Chemiluminescent western detection was performed with C-digit instrument (LI-COR, Inc. Burlington, ON, Canada) and Clarity™ western ECL substrate reagents (Bio-Rad, Cat. #1705061, CA, USA).

RNA Isolation

Total RNA was extracted from Calu-3 infected and non-infected cells at the 24 h, 48 h and 72 h time points, using RNA Easy kit (Qiagen, Cat. #74106, Toronto, Ontario, Canada) following the manufacturer's recommendations. All RNA samples were treated with DNase I, quantified with the NanoDrop™ 2000 Spectrophotometer (Thermo Scientific™, Cat #ND-2000) and kept at -80°C for subsequent experiments.

Illumina Nextseq Sequencing of Cells Infected With SARS-CoV-2 Viruses

Total RNA from each biological sample was used to prepare the miRNA sequencing library, which included the following steps: 1) 3'-adapter ligation; 2) 5'-adapter ligation; 3) cDNA synthesis; 4) PCR amplification; 5) size selection of ~130-150 bp PCR amplified fragments. The libraries were denatured as single-

 doi:10.20944/preprints202208.0340.v1

stranded DNA molecules, captured on Illumina flow cells, amplified in situ as clusters and finally sequenced for 50 cycles on Illumina Nextseq per the manufacturer's instructions. The method, the experimental workflow and the flowchart of data analysis are detailed in our previous report [26].

More than 6 million raw sequences were generated as clean reads from Illumina Nextseq by real-time base calling and quality filtering. The adapter-trimmed reads above 16 nt varied between 41 and 69% on average (**Supplementary Table S1**). Based on Novoalign software, 27% to 54% of these adapter-trimmed reads (>16 nt) were aligned to known human pre-miRNA in miRBase21 (**Supplementary Table S1**) and their read length distribution in Calu-3 cells infected cells highlighted an abundance of 22 nt sequences generally corresponding to the average size of miRNAs (**Supplementary Figure S1**). The status (infected vs uninfected) and the stage (24 h vs 72 h) of infection did not significantly alter the number of reads obtained (**Supplementary Figure S1**).

RT-qPCR

Detection of host mRNA targets and SARS-CoV-2 genome. RNA extracted from host infected and non-infected cells was converted to cDNA with the HiFlex miScript II RT Kit (Qiagen, Cat. #218160, MD, USA) following the manufacturer's protocol. After dilution of the cDNA (1/10), qPCR was performed using the SSoAdvanced SYBR Green mix (Bio-Rad, Cat. #1725271, CA, USA). The primers (Integrated DNA Technologies; sequences listed in **Supplementary Table S2**), used at 1 μM final concentration, were designed with Primer-BLAST tools [27] and the best annealing temperature was chosen for each primer pair following a temperature gradient test. The qPCRs were performed using the StepOne™ Real-Time PCR System (Applied Biosystems, Cat. #4376357) and data obtained (from StepOne™ Software, v2.3) were normalized with reference gene (actin beta, ACTB) and reported to the controls (non-infected condition). The relative quantitation was calculated using the ddCt method [28].

Detection of host miRNAs. To monitor miR-1246 (GeneGlobe ID - YP00205630) and miR-1290 (GeneGlobe ID - YP02118634) we designed specific and sensitive (optimized with LNA technology [29]) microRNA primer sets of the miRCURY LNA miRNA Custom PCR Assay (Qiagen, Cat. #339317, MD, USA). qPCR was performed using diluted cDNA (1/10) and the miRCURY LNA SYBR Green PCR Kit (Qiagen, Cat. #339346, MD, USA) supplemented with ROX dye (Qiagen, Cat. #339346, MD, USA). The qPCRs were performed using the StepOne™ Real-Time PCR System (Applied Biosystems, Cat. #4376357). The U6 small nuclear RNA (RNU6) was used as a reference gene. Also, UniSp6 RNA spike-in was used for cDNA synthesis and PCR amplification normalization as described previously [30].

Plasmid Constructs

The wild-type (WT) sequences of ACE2 3'-UTR (NCBI accession number: NM_001371415.1) and a mutated version were designed by using gBlocks® gene fragments (Integrated DNA Technologies, Inc., Coralville, IA, USA). These sequences of 873 nt of ACE-2 3'UTR were introduced downstream of the Renilla luciferase (Rluc) reporter gene the XhoI/NotI cloning sites of the psiCHECK2 vector (Promega, Madison, WI, USA). The details of the construction strategy have been previously described [30] and are summarized in **Supplementary File SA**. All the constructs were independently confirmed by DNA sequencing at the Plateforme de Séquençage et Génotypage des Génomes (Centre de Recherche du CHU de Québec – CHUL, QC, Canada).

 doi:10.20944/preprints202208.0340.v1

Cell Transfection and Dual-Luciferase Assay

Cell transfection and dual-luciferase assay were performed as described previously, with slight modifications [30]. Calu-3 cells were cultured in 6-well plates (300 000 cells per well) and transfected the following days at 70–80% with miRIDIAN miRNA-1246 and/or miRIDIAN miR-1290 mimics (Dharmacon, Horizon Discovery, Cat #C-301373-00-0002; Cat #C-301344-00-0002, Lafayette, CO, USA) and psiCHECK2 plasmids (WT or mutant). 48 h after transfection, cells were washed with PBS and lysed with 500 µL of the passive lysis buffer (Promega, Cat. #E1980, WI, USA). Luciferase activities were measured using the Dual-Luciferase® Reporter Assay System (Promega, Cat. #E1980, WI, USA) in a luminometer (TECAN INFINITE M1000 PRO), according to manufacturer's instructions. Renilla luciferase (Rluc) expression was reported relatively to the expression of the internal control Firefly luciferase (Fluc). Rluc expression was further normalized to the control in which cells were co-transfected with unrelated negative control miRNA mimic, referred to elsewhere as mock control. All assays were conducted in biological and technical triplicates in a 96-well format.

Statistical Analysis of qPCR Data

The statistical method used in each case is mentioned under figures. All statistical analyses were performed using GraphPad Prism version 9.3.1 (GraphPad Software, Inc., La Jolla, CA, USA), with statistical significance set at $p < 0.05$.

Preprints (www.preprints.org) | NOT PEER-REVIEWED | Posted: 18 August 2022 doi:10.20944/preprints202208.0340.v1

Results

1. SARS-CoV-2 replication in Calu-3 cells

To profile the miRNome of lung epithelial cells following SARS-CoV-2 infection, we infected Calu-3 cells with the clinical isolate, SB3 (PMID 32558639). Virus replication was confirmed by monitoring the SARS-CoV-2 nucleocapsid (N) transcript and protein expression levels. SARS-CoV-2 nucleocapsid is an abundant viral RNA-binding protein essential for SARS-CoV-2 genome packaging and is highly expressed in infected cells [31]. SARS-CoV-2 nucleocapsid mRNA and protein were specifically detected within infected cells by RT-qPCR and western blotting, respectively (**Figure 1**). Between 24 h and 48 h post-infection, N mRNA levels were approximately the same, whereas in the late phase of infection (72 h), they increased eight-fold (**Figure 1A**). Meanwhile, N protein levels remained relatively stable over time (**Figure 1B**).

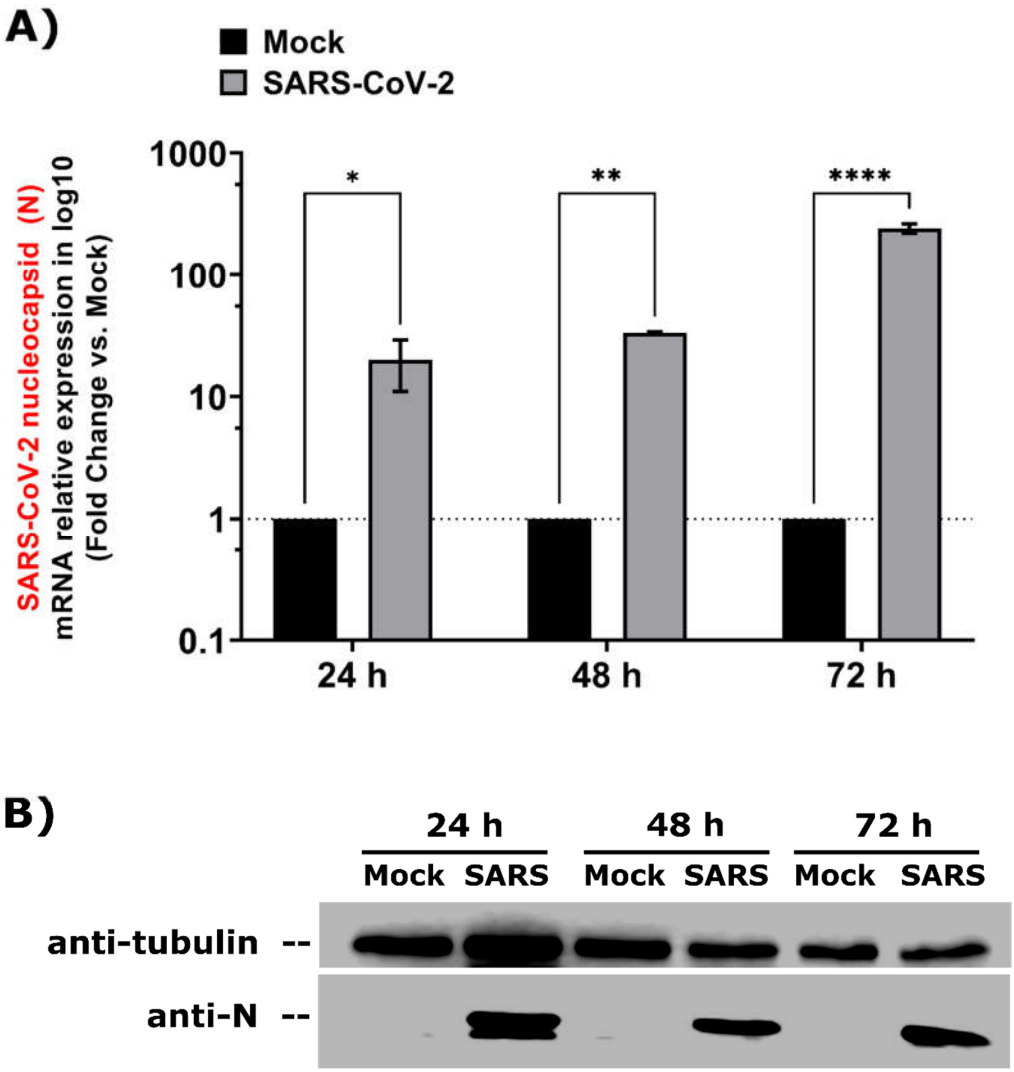

Figure 1. SARS-CoV-2 replication in Calu-3 cells. SARS-CoV-2 *nucleocapsid* gene (N) expression was monitored upon SARS-CoV-2 infection in Calu-3 cells by RT-qPCR (A) using specific primers and Western blot (B) using anti-N and anti-Tubulin (control) antibodies. qPCR data were normalized with a reference gene (Actin beta, *ACTB*), reported to mock (unrelated negative control), and expressed with a relative quantitation method (ddCT). **Statistical analysis.** All data (A) presented were calculated from three

biological replicates (n = 3) measurements ± SD. The ordinary two-way analysis of variance (ANOVA) and Šídák's multiple comparisons test were used for statistical analysis. Statistically significant differences (fold change vs. mock) are indicated by stars (*): * p < 0.05; ** p < 0.01; *** p < 0.001; **** p < 0.0001.

SARS-CoV-2 Infection May Stimulate Peptidases Involved in Virus Entry

Next, we performed a transcriptional analysis by qPCR to assess how SARS-CoV-2 modulates the expression of host genes that are involved in the virus entry. We were interested in the SARS-CoV-2 mediated transcriptional modulation of key peptidases necessary for cellular entry, including ACE-2, TMPRSS2, ADAM-17 and Furin [6,32,33]. These proteases were all significantly upregulated at the early stage of infection (24 h, **Figure 2**) compared to mock-infected cells. Their expression level reached normal levels at the 48 h and 72h time points, except for ACE-2 and ADAM17 which remained upregulated even in the late phase of infection (72 h).

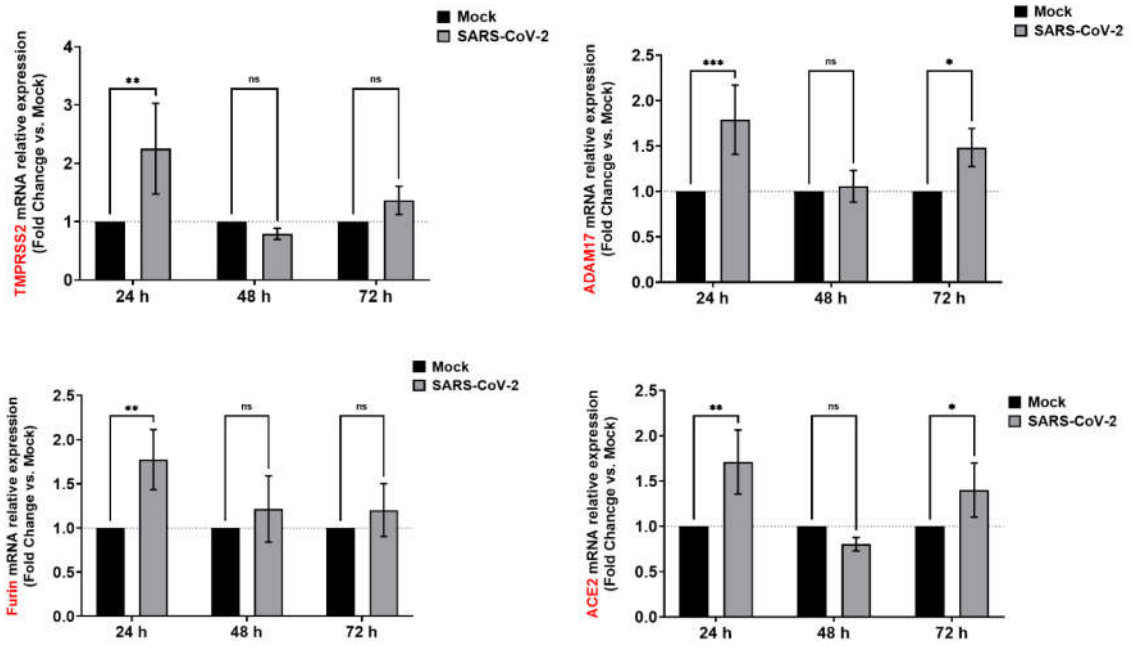

Figure 2. SARS-CoV-2 regulates host carboxypeptidases involved in the release of ACE2 ectodomain from the cell surface and in the entry of the virus into the cells. mRNA levels of *ACE2, TMPRSS2, ADAM17 and Furin* genes were monitored by RT-qPCR (relative expression) upon SARS-CoV-2 infection in Calu-3 cells. qPCR data were normalized with a reference gene (Actin beta, *ACTB*), reported to mock and expressed with a relative quantitation method (ddCT). Statistical analysis. All data presented were calculated from three biological replicates (n = 3) measurements ± SD. The ordinary two-way analysis of variance (ANOVA) and Šídák's multiple comparisons test were used for statistical analysis. Statistically significant differences (fold change vs mock) are indicated by stars (*): * p < 0.05; ** p < 0.01; *** p < 0.001; **** p < 0.0001.

SARS-CoV-2 infection may lead to prompt activation of the innate immune response and triggers fundamental cellular processes

We next monitored the expression of Interferon 1 beta (IFN1β) to assess the innate immune response and the levels of Interlukin-6 (IL-6) and C-X-C motif chemokine ligand 10 (CXCL10) to assess the levels of inflammatory cytokines. The expression of these genes is altered following SARS-CoV-2 infection [34,35].

Preprints (www.preprints.org) | NOT PEER-REVIEWED | Posted: 18 August 2022 doi:10.20944/preprints202208.0340.v1

As previously observed with peptidases, IL-6, IFN1β and CXCL10 were significantly upregulated at 24 h with a fold increase of about 2, then returned to normal at 48 h and 72 h except for IFN1β which remained elevated at 72 h (**Figure 3**). We also observed that the genes involved in fundamental cellular processes such as *SOCS4, AKT, NOTCH* and *WNT* [36–39]) were also upregulated in the early stages of infection (**Supplementary Figure S2**).

Taken together, these results suggest that SARS-CoV-2 induces an early and transient response of host genes involved in global regulation, consistent with our previous observations [25].

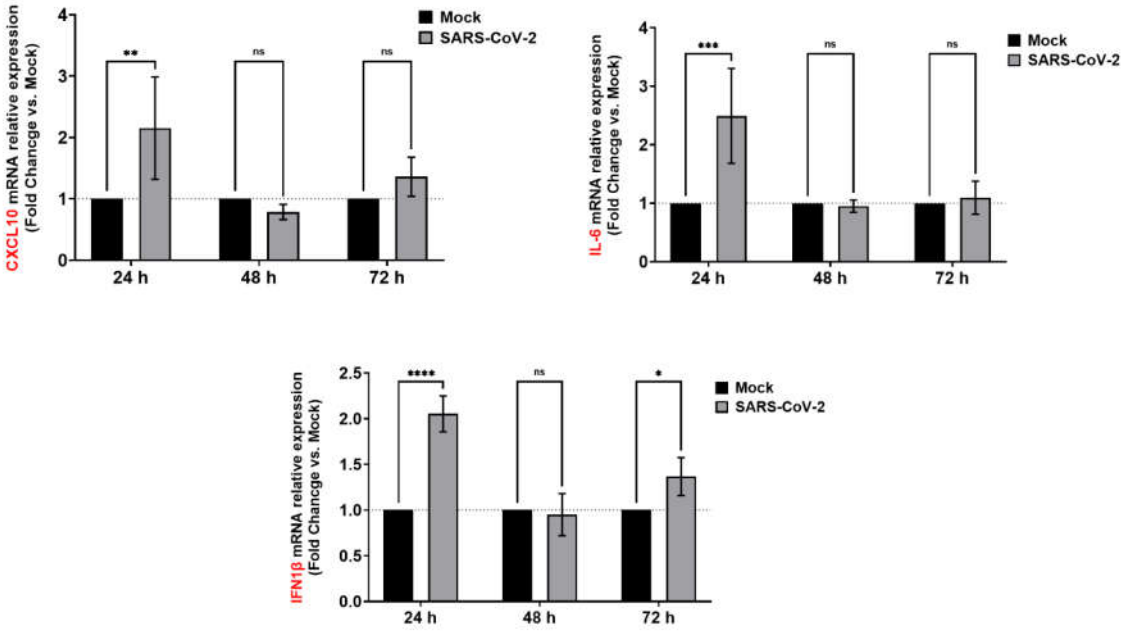

Figure 3. SARS-CoV-2 may regulate several predicted host mRNA targets involved in innate immune response. mRNA levels of *Il-6*, *IFN1β*, *CXCL10* genes were monitored by RT-qPCR (relative expression) upon SARS-CoV-2 infection in Calu-3 cells. qPCR data were normalized with a reference gene (Actin beta, *ACTB*), reported to mock, and expressed with a relative quantitation method (ddCT). **Statistical analysis.** All data presented were calculated from three biological replicates (n = 3) measurements ± SD. The ordinary two-way analysis of variance (ANOVA) and Šídák's multiple comparisons test were used for statistical analysis. Statistically significant differences (fold change vs control) are indicated by stars (*): * $p < 0.05$; ** $p < 0.01$; *** $p < 0.001$; **** $p < 0.0001$.

SARS-CoV-2 infection modulates the Renin Angiotensin Aldosterone System (RAAS)

In addition to being the main entry point identified for the virus into the cell, angiotensin-converting enzyme 2 (ACE2) is also a main player of the renin-angiotensin-aldosterone-system (RAAS) with angiotensinogen (AGT), angiotensin-converting enzyme (ACE) and renin [40].

Quantitative PCR analysis of these genes (**Figure 4**) showed a significant increase of ACE and AGT at 24 hours, while renin was drastically downregulated (more than 50% reduction) at the same time. As with the previous data, neither of the aforementioned genes was significantly modulated at 48 h. At 72 h, renin, but not ACE or AGT, not only recovered its levels but also was upregulated by 2-fold compared to baseline expression.

Preprints (www.preprints.org) | NOT PEER-REVIEWED | Posted: 18 August 2022 doi:10.20944/preprints202208.0340.v1

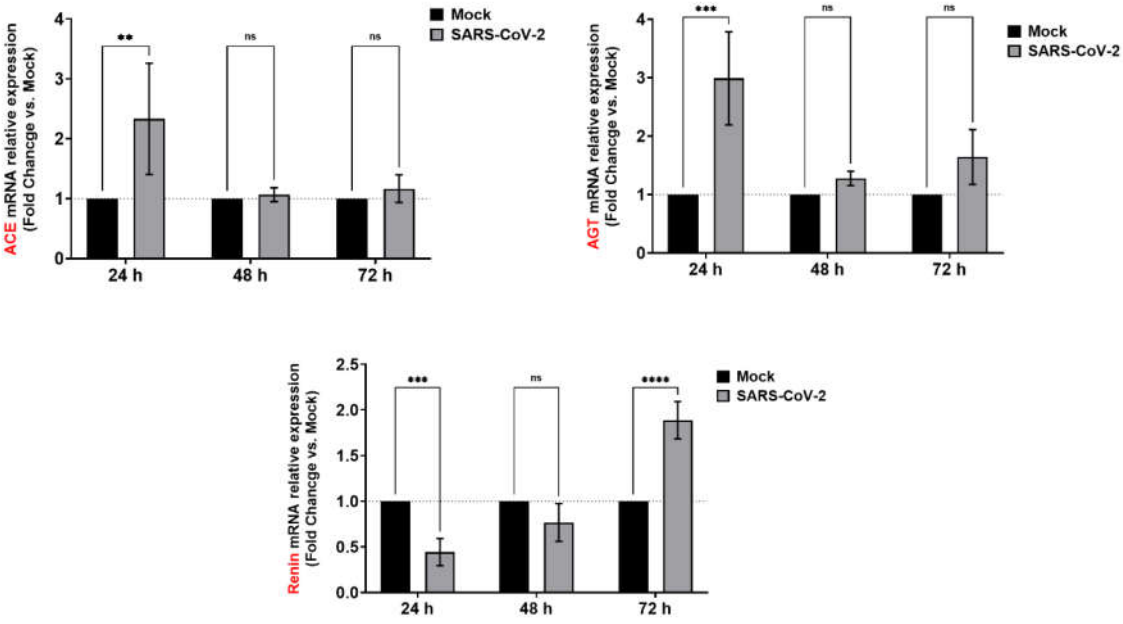

Figure 4. SARS-CoV-2 may regulate several predicted host targets involved in *Renin*-Angiotensin System (RAS). mRNA levels of *ACE*, *AGT* and *Renin* genes were monitored by RT-qPCR (relative expression) upon SARS-CoV-2 infection in Calu-3 cells. qPCR data were normalized with a reference gene (Actin beta, *ACTB*), reported to mock, and expressed with a relative quantitation method (ddCT). **Statistical analysis.** All data presented were calculated from three biological replicates (n = 3) measurements ± SD. The ordinary two-way analysis of variance (ANOVA) and Šídák's multiple comparisons test were used for statistical analysis. Statistically significant differences (fold change vs control) are indicated by stars (*): * $p < 0.05$; ** $p < 0.01$; *** $p < 0.001$; **** $p < 0.0001$.

SARS-CoV-2 Infection Does Not Alter the Relative Abundance of miRNAs

We next investigated how the miRNome, very often overshadowed by the general focus on the proteome, is modulated in the context of SARS-CoV-2 infection, and how this modulation could explain our previous observations or might contribute to the widely described pathogenesis of SARS-COV-2. Expression profiling of miRNAs at the 24 h and 72 h were performed in SARS-CoV-2-infected Calu-3 cells using RNA-Seq. Expression profiling of miRNAs (**Figure 5**) revealed that infection at the early or late stage has little or no effect in terms of their order of abundance. Specifically, the 20 most abundant miRNAs and their relative proportions were almost the same with or without SARS-CoV-2 infection (**Figure 5**).

Preprints (www.preprints.org) | NOT PEER-REVIEWED | Posted: 18 August 2022 doi:10.20944/preprints202208.0340.v1

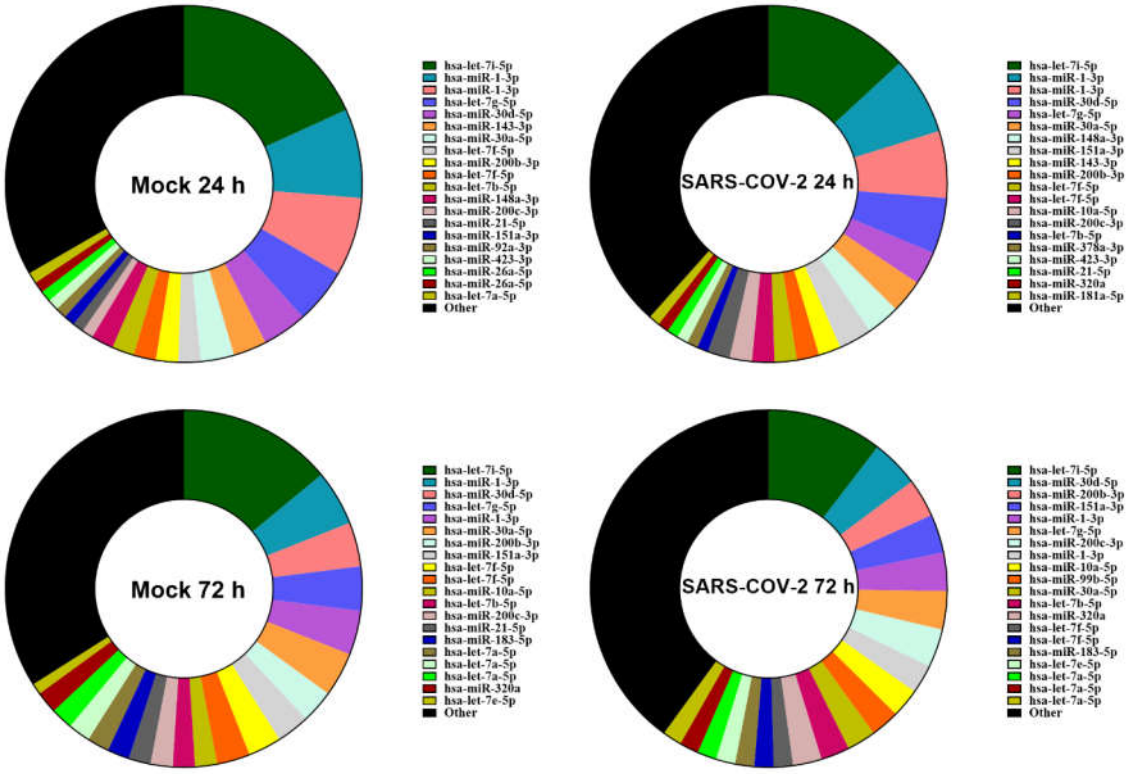

Figure 5. miRNA expression profiling of Calu-3 cells infected or not with SARS-CoV-2 virus. Circular diagram representing the 20 most abundant microRNAs in each experimental condition (Mock- or SARS-CoV-2- infected, 24 h and 72 h) along with other microRNAs and their relative proportions assessed by RNA-Seq. The ranking was based on the normalized tag number of miRNAs averaged from 3 biological replicates.

A finite number of miRNAs are differentially expressed upon SARS-CoV-2 Infection

As there was no significant change in the relative abundance of miRNAs, we were interested in the differentially expressed (DE) miRNAs, i.e., how many miRNAs were upregulated, downregulated, and how many remained unaltered. While comparing infected with non-infected samples (n=3), we selected as the DE miRNAs those having fold changes greater than or equal to 1.5 and P-values less than or equal to 0.05.

Differences in miRNA expression upon SARS-CoV-2 infection were illustrated by a scatter plot (**Figure 6**) which displayed a very strong correlation (r=0.9904 at 24 h and 0.9918 at 72 h) between miRNA profiles from both experimental conditions (infected vs uninfected). At 24 h, 119 miRNAs were upregulated while 16 were downregulated. On the other hand, at 72 h, 87 miRNAs were upregulated while 26 were downregulated. The non-DE miRNAs were 1013 at 24 h versus 1154 at 72 h. When expressed as relative percentages (**Supplementary Figure S3**), 88% and 91% were non-differentially expressed at 24 h and 72 h post-infection, respectively.

Preprints (www.preprints.org) | NOT PEER-REVIEWED | Posted: 18 August 2022 doi:10.20944/preprints202208.0340.v1

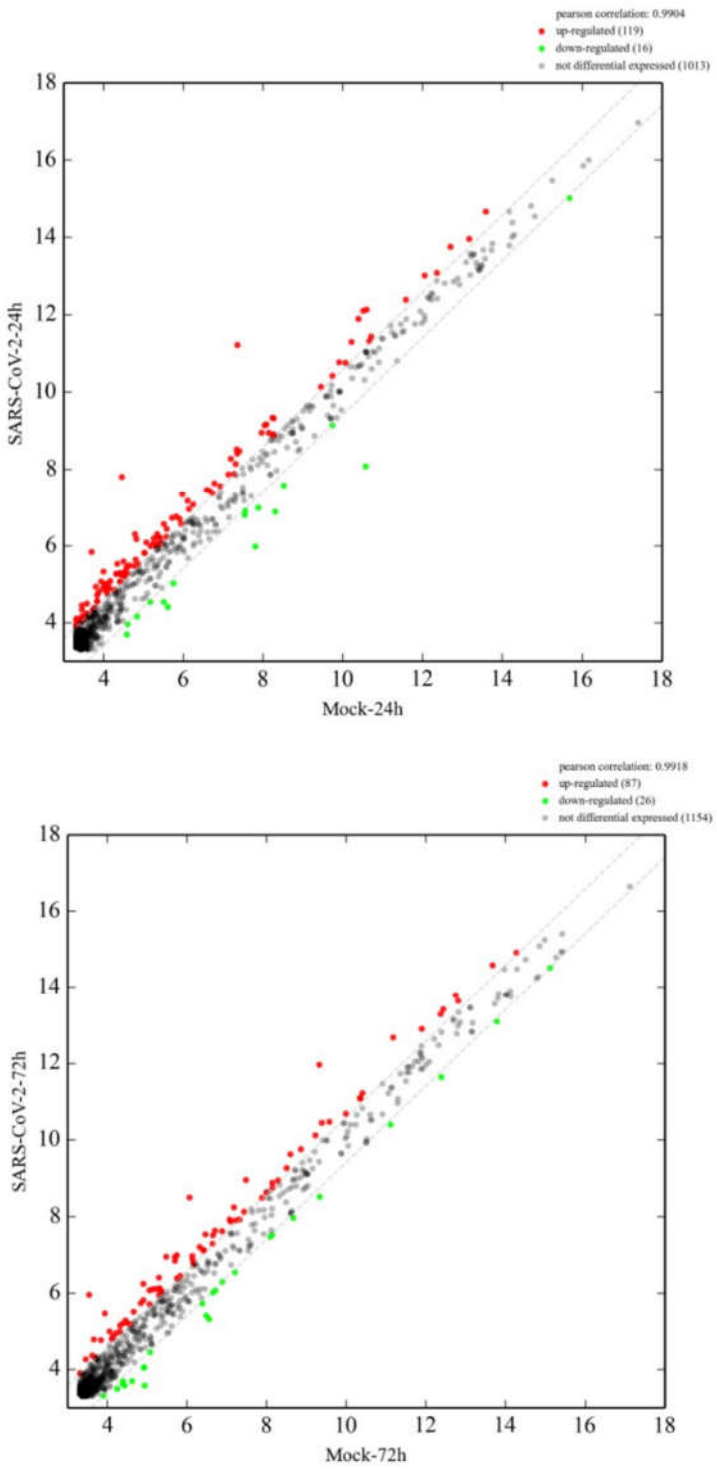

Figure 6. Scatter plot of differentially expressed miRNAs of Calu-3 cells infected or not with SARS-CoV-2 virus. Scatter plot showing up-regulated (red spots), downregulated (green spots) and non-differentially expressed miRNAs (black spots) at 24 h and 72 h post-infection.

SARS-CoV-2 Infection Induces Consistent Upregulation of miR-1246 and miR-1290

Preprints (www.preprints.org) | NOT PEER-REVIEWED | Posted: 18 August 2022 doi:10.20944/preprints202208.0340.v1

To further consolidate our observations, the DE miRNAs were subjected to two additional analytical plots: volcano plot (**Figure 7**) showing statistical significance versus magnitude of change and a heat map (**Figure 8**) showing the hierarchical clustering of DE miRNAs. As shown by the correlation plot (**Figure 6**), the volcano plot (**Figure 7**) confirmed the very low number of miRNAs which were differentially expressed following SARS-CoV-2 infection (only 69 miRNAs versus 1079 non-DE at 24 h and 25 miRNAs versus 1242 non-DE at 72 h).

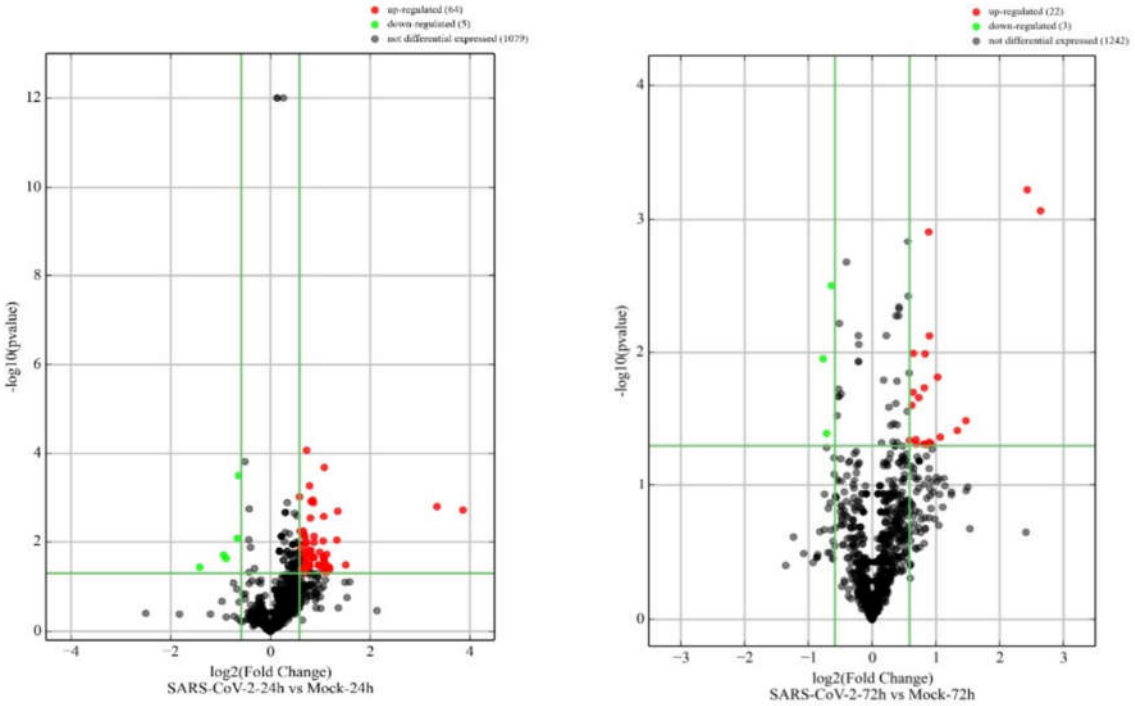

Figure 7. Volcano plot of differentially expressed miRNAs. Plots depicting the magnitude (log 2 reporting fold change, FC, x-axis) and significance (− log 10 adjusted P value, y-axis) of differentially expressed miRNAs between Mock and SARS-CoV-2-infected Calu-3 cells A) 24 h and B) 72 h post-infection. The green, red, and black spots represent upregulated, downregulated, and non-differentially expressed miRNAs, respectively. The statistical significance threshold ($P \leq 0.05$) is illustrated by the horizontal green line and the threshold of fold change (log 2 FC > 1 or < − 1) by the two vertical green lines.

The heat map listing differentially expressed miRNAs from 3 independent samples (3 infected, 3 uninfected controls) at 24 h and 72 h particularly highlights two miRNAs that are upregulated upon SARS-CoV-2 infection: miR-1246 and miR-1290 (**Figure 8**). **Tables 1** and **2** summarize the fold change along with the p-value and False Discovery Rate (FDR) of the top 10 up- and down-regulated miRNAs after infection at 24 h and 72h, respectively. miR-1246, the most upregulated of Calu-3 miRNAs, showed a fold change of 14.55 (p-value =0.0019; FDR=0.1245) at 24 h and 6.23 (p-value = 0.0008; FDR= 0.4654) at 72 h post-infection (**Table 1**). miR-1290, which was ranked second, was upregulated by 10.15-fold (p-value = 0.0016; FDR= 0.1245) and 5.39 (p-value = 0.0005; FDR= 0.4654, **Table 1**) at 24 h and 72 h, respectively. miR-196b-5p and miR-196a-5p, and miR-3924 and miR-30e-5p, were the most downregulated at 24 h and 72 h, respectively (**Table 2**).

Preprints (www.preprints.org) | NOT PEER-REVIEWED | Posted: 18 August 2022 doi:10.20944/preprints202208.0340.v1

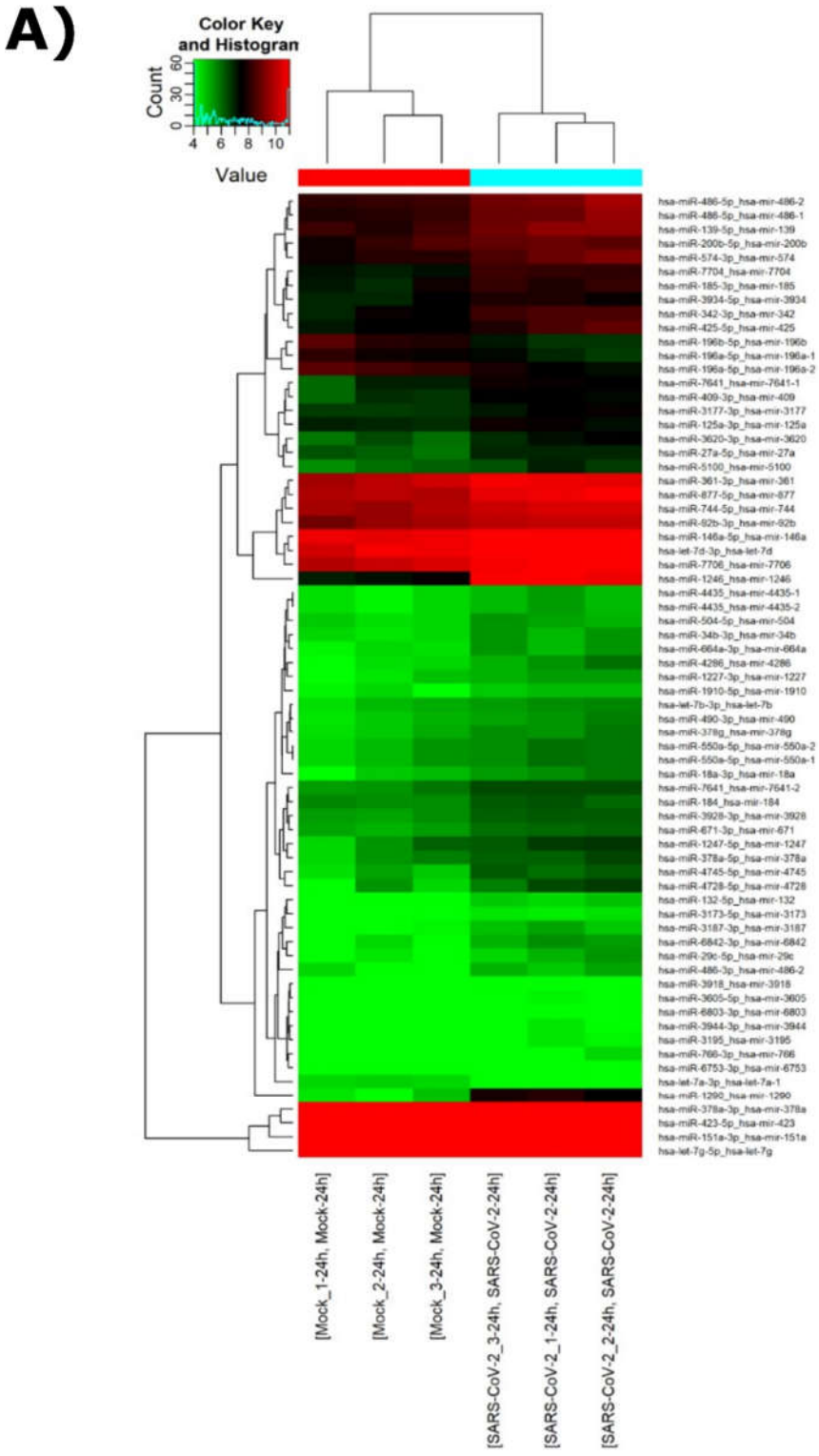

Preprints (www.preprints.org) | NOT PEER-REVIEWED | Posted: 18 August 2022 doi:10.20944/preprints202208.0340.v1

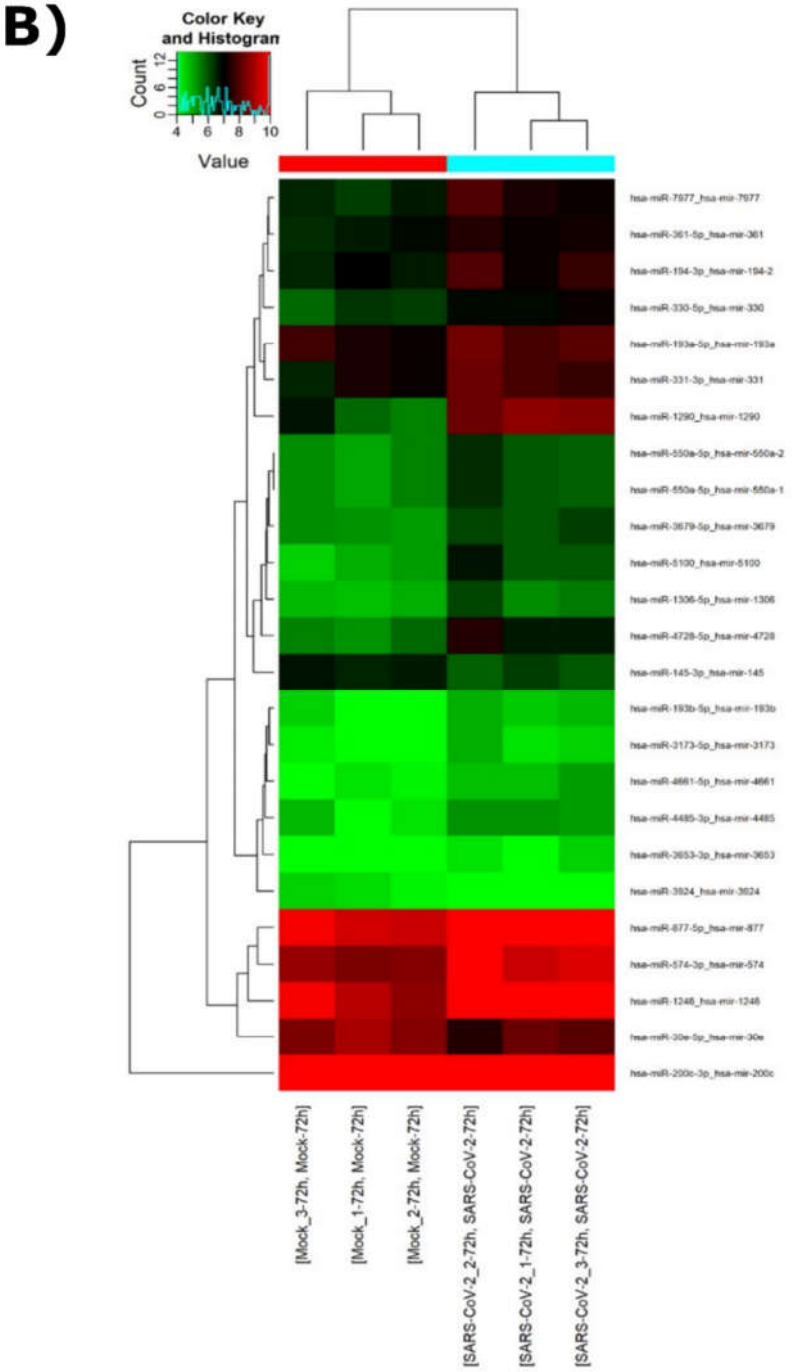

Figure 8. Heat map and hierarchical clustering of differentially expressed miRNAs. miRNA expression levels are illustrated using a histogram and color key. The upper dendrogram illustrates the clustering of samples (n=3) infected or not (mock) with SARS-CoV-2 at A) 24 h and B) 72 h post-infection. The left dendrogram illustrates the clustering of miRNAs differentially expressed and listed in the left vertical axis. Each row represents a miRNA, and each column represents a sample.

Table 1. Top 10 upregulated miRNAs in Calu-3 cells at 24 h and 72 h post-SARS-CoV-2 infection, compared to uninfected control (Mock). FDR= False Discovery Rate.

Preprints (www.preprints.org) | NOT PEER-REVIEWED | Posted: 18 August 2022 doi:10.20944/preprints202208.0340.v1

Mature miRNAs	Fold change	P-value (unpaired)	FDR
SARS-CoV-2-24 h vs Mock-24 h			
hsa-miR-1246	14,550813	0,001936356	0,124553971
hsa-miR-1290	10,151515	0,001616931	0,124553971
hsa-miR-4728-5p	2,855422	0,032727219	0,340049232
hsa-miR-4745-5p	2,552941	0,002060005	0,124553971
hsa-miR-6842-3p	2,520833	0,00909142	0,246889589
hsa-miR-4286	2,278689	0,040817409	0,366081138
hsa-miR-425-5p	2,263918	0,036130815	0,348556098
hsa-miR-29c-5p	2,195652	0,047218269	0,408413103
hsa-miR-3187-3p	2,190476	0,018900103	0,293985775
hsa-miR-486-5p	2,147124	0,031260241	0,340049232
SARS-CoV-2-72 h vs Mock-72 h			
hsa-miR-1246	6,234131	0,000859555	0,465454769
hsa-miR-1290	5,393035	0,000599562	0,465454769
hsa-miR-4728-5p	2,768657	0,032469057	0,605339181
hsa-miR-5100	2,522222	0,038432487	0,605339181
hsa-miR-7977	2,098113	0,043036275	0,605339181
hsa-miR-574-3p	2,036113	0,015325686	0,605339181
hsa-miR-194-3p	1,897764	0,048234042	0,605339181
hsa-miR-877-5p	1,861196	0,007521499	0,605339181
hsa-miR-1306-5p	1,860465	0,046973589	0,605339181

Table 2. Top 10 downregulated miRNAs in Calu-3 cells at 24 h and 72 h post-SARS-CoV-2 infection, compared to uninfected control (Mock). [No other miRNAs meeting the criteria other than the ones listed in this table were identified. FDR= False Discovery Rate. Therefore, the top10 does not contain 10 miRNAs.].

Mature miRNA	Fold change	P-value (unpaired)	FDR
SARS-CoV-2-24 h vs Mock-24 h			
hsa-miR-196b-5p	0,374473	0,036770814	0,351774119
hsa-miR-196a-5p	0,521818	0,01962821	0,293985775
hsa-miR-196a-5p	0,540311	0,023390933	0,308652771
hsa-let-7g-5p	0,633044	0,008259531	0,246889589
hsa-let-7a-3p	0,643836	0,000312666	0,05127724
SARS-CoV-2-72 h vs Mock-72 h			
hsa-miR-3924	0,587302	0,011169221	0,605339181
hsa-miR-30e-5p	0,609796	0,040388915	0,605339181
hsa-miR-145-3p	0,642384	0,003165844	0,605339181

To confirm our observations and to validate our RNA-Seq data, we measured the expression level of miR-1246 and miR-1290 by qPCR on the same biological samples (**Figure 9**). Both miR-1246 and miR-1290 were found significantly upregulated at the two time points (24 h and 72 h). Following the same trend as in RNA-seq data, miR-1246 showed higher fold change than miR-1290 (**Figure 9**). At 48 h, a condition not included in our RNA-Seq analysis, only miR-1246 appears significantly upregulated (1.56 fold).

Preprints (www.preprints.org) | NOT PEER-REVIEWED | Posted: 18 August 2022 doi:10.20944/preprints202208.0340.v1

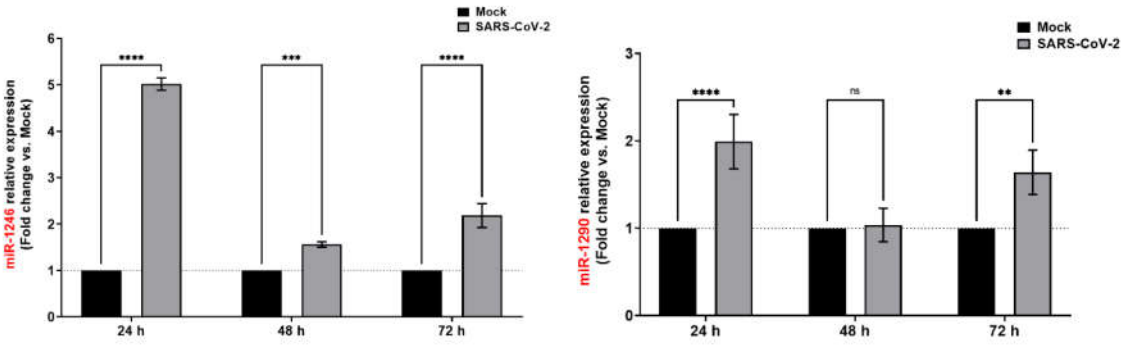

Figure 9. Validation of miR-1246 and miR-1290 upregulation (RNA-Seq data) by qPCR. miR-1246 and miR-1290 were monitored by RT-qPCR upon SARS-CoV-2 infection in Calu-3 cells. qPCR data were normalized with a reference gene (U6 snRNA), reported to mock, and expressed with a relative quantitation method (ddCT). **Statistical analysis.** All data presented were calculated from three biological replicates (n = 3) measurements ± SD. The ordinary two-way analysis of variance (ANOVA) and Šídák's multiple comparisons test were used for statistical analysis. Statistically significant differences (fold change vs control) are indicated by stars (*): * $p < 0.05$; ** $p < 0.01$; *** $p < 0.001$; **** $p < 0.0001$.

miR-1246 Targets and Regulates ACE2

Ubiquitously expressed at varying levels, ACE2 is known to be the major cell entry receptor for SARS-CoV-2 [41,42]. The significant upregulation of miR-1246 led us to investigate whether it could affect ACE2 expression.

To assess this possible correlation, we used the dual luciferase reporter assay and co-transfected Calu-3 cells with miR-1246 and a psiCHECK2 plasmid which carries a portion (approximately 900 base pairs, see details in Materials and Methods section) of the 3'UTR of ACE2 (wild-type or mutant) bearing inherent in silico predicted sites of miR-1246 (**Figure 10**). In the absence of miR-1246 mimic, the normalized luciferase expression was reduced by about 15% both in the plasmid carrying the 3'UTR wild-type of ACE2 and the mutated version suggesting the presence of elements with downregulatory properties in the 3'UTR of ACE2. When miR-1246 was added at increasing doses (25 to 100 nM), a 30 to 40% decrease in luciferase expression was observed for the plasmid with ACE2 wild type 3'UTR (**Figure 10**). On the other hand, plasmid with ACE2 mutated 3'UTR showed only 10% decrease of luciferase signal. miR-1246 thus appears to be a direct and specific regulator of the ACE2 mRNA. Similarly, we measured the expression of luciferase after the addition of miR-1290 alone (**Supplementary Figure S4**) or in combination with miR-1246 (**Supplementary Figure S5**). miR-1290 is the exact copy of miR-1246 without two adenine nucleotides on the 5' side. However, it did not seem to induce any repression of luciferase expression (**Supplementary Figure S4**). The mix of miR-1246 and miR-1290 did not trigger stronger repression of luciferase expression compared to miR-1246 alone (**Supplementary Figure S5**). The contribution of miR-1290 was negligible, reinforcing the hypothesis of a specific interaction between miR-1246 and the 3'UTR of ACE2.

Preprints (www.preprints.org) | NOT PEER-REVIEWED | Posted: 18 August 2022 doi:10.20944/preprints202208.0340.v1

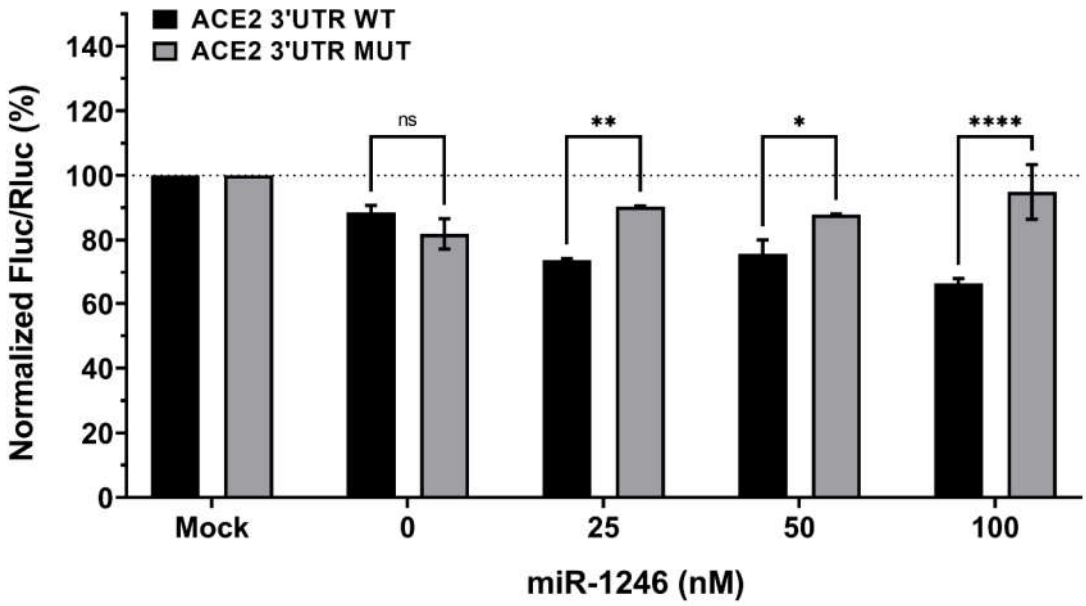

Figure 10. Modulation of human ACE2 mRNA by hsa-miR-1246. Calu3 cells were co-transfected with Homo sapiens (hsa) human miR-1246 mimic (0, 25, 50, and 100 nM) and a psiCHECK2 reporter construct (50 ng; see **Supplementary File SA**), in which the Rluc reporter gene was coupled with wild-type (WT) or mutated (MUT) human ACE2 3′ Untranslated Region (UTR). An unrelated, negative miRNA control (Mock) was used for normalization, in addition to the internal normalizer Fluc. "0 nM" corresponds to the transfection reagent-only control. Statistical analysis: Data were calculated from three biological replicates and expressed as means ± SD. The two-way analysis of variance (ANOVA) and Šídák's multiple comparisons test were used, and statistically significant differences (fold change WT vs MUT) are indicated as follows: * $p < 0.05$; ** $p < 0.01$; *** $p < 0.001$; **** $p < 0.0001$; ns, nonsignificant.

GO and KEGG analyses of differentially expressed miRNAs

In an attempt to understand how the dysregulation observed at the level of miRNAs in host cells would contribute to SARS-CoV-2 pathogenesis, symptoms or host defense against SARS-CoV-2 infection, we subjected the above DE miRNAs to KEGG and GO analysis.

"RAS and MAPK signaling pathway", the "cholinergic synapse" and "endocytosis", were among the significantly enriched KEGG pathways related to genes targeted by the upregulated miRNAs (**Figure 11A**), in both early (24 h) and late stages (72 h) of infection. Some KEGG Pathways were found uniquely at 24 h ("aldosterone synthesis and secretion") or 72 h ("neurotrophin signaling pathway").

"RAS and MAPK pathways" were also found in significantly enriched KEGG pathways of downregulated miRNAs but with half as many genes involved (**Figure 11B**). "PI3K-AKT, AMPK, AGE-RAGE signaling pathways" and "cell cycle" were among the significantly and specifically enriched KEGG pathways related to genes targeted by downregulated miRNAs at 24 h. "Renin secretion", "regulation of actin cytoskeleton" and "glutamatergic synapse" were among the enriched KEGG pathways at 72 h.

Furthermore, using the GO knowledge base (biological process, cellular component, and molecular function) we identified the main pathways in which DE miRNAs may be involved (**Supplementary Figures S6 & S7**). Upon SARS-CoV-2 infection, the upregulated miRNAs seemed to affect several biological

Preprints (www.preprints.org) | NOT PEER-REVIEWED | Posted: 18 August 2022 doi:10.20944/preprints202208.0340.v1

processes we mention, among others, "regulation of cellular processes and localization" and "signaling"; the cellular components such as "intracellular" and "cytoplasm"; and the molecular function such as "protein binding" and "transcription factor activity" (**Supplementary Figure S6**). For the downregulated miRNAs, among other terms, the 3 GO aspects emphasized "metabolic process" for the biological process, "intracellular" for the cellular components and "protein binding" for the molecular functions (**Supplementary Figure S7**).

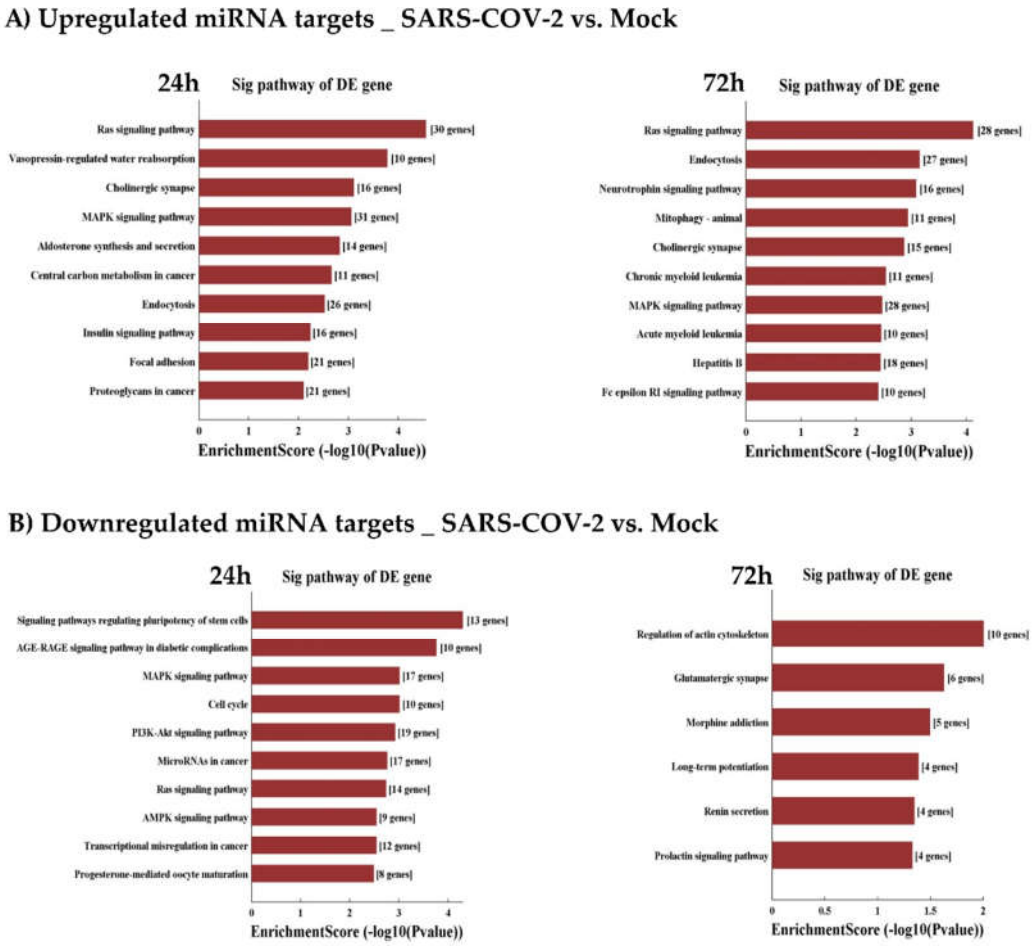

Figure 11. Enrichment score values of the top 10 enrichment pathways following SARS-CoV-2 infection vs Mock. The bar plot shows the top 10 significantly enriched KEGG pathways of genes targeted by A) upregulated and B) downregulated miRNAs at 24 h and 72 h post-infection.

 doi:10.20944/preprints202208.0340.v1

Discussion

In this study we investigated COVID-19 from the perspective of noncoding RNAs, in particular miRNAs. The challenge was, as in our previous works on HIV/AIDS virus [43,44], the Ebola virus [26,30] and the Hepatitis B virus [45], to understand how SARS-CoV-2 modulates the host miRNA profile during infection and eventually whether it encodes expressed viral miRNAs involved in pathogenesis.

Our RNA-Seq data and the subsequent bioinformatics analyses enabled us to identify more than 1000 host miRNAs but none from the viral genome (using a pipeline similar to the one we used for Ebola [30]). Compared with the uninfected controls, the volcano plot showed that 64 and 22 host miRNAs were upregulated at 24 h and 72 h respectively, while only 5 and 3 host miRNAs were downregulated at 24 h and 72 h respectively in the infected Calu-3 cells. Similar to our studies on Ebola virus infection [26], very few miRNAs were modulated by the presence of the virus, the vast majority remaining non-differentially expressed. This phenomenon could also be the result of an evolutionary adaptation of viruses allowing them to evade miRNAs [15].

In a previous study conducted by a team in Toronto in human lung epithelium 24 h after SARS-CoV-2 infection, the analysis of differentially expressed miRNAs revealed that only 45 miRNAs were differentially expressed [23]. In peripheral blood of ten COVID-19 patients, Li et al. found a total of 73 human miRNAs to be differentially expressed [21]. Other studies involving other viruses also reported similar findings [46,47].

Consequently, in the context of SARS-CoV-2 infection or RNA viruses like Ebolavirus, there seems to be a general tendency for specific, targeted and pool-limited regulation of miRNAs. SARS-CoV-2 may use pathways that minimally affect miRNA-related cellular processes. In fact, miRNAs appear to be more involved in pathways conferring robustness to biological processes than in defense against foreign nucleic acid [48]. Further studies are warranted to clarify the role of DE miRNAs, however, they may be pivotal in the control of viral tropism [49] and may serve as potential informative biomarkers [50]. From another perspective, the susceptibility of the lung epithelia to infection could arise from the lack of important miRNA-associated protective mechanism [23,51].

GO and KEGG analyses show that essential pathways are affected by the DE miRNAs upon SARS-CoV-2 infection. This was the case for RAS and MAPK signalling pathways which are involved in all fundamental processes of the cell, such as transcription, differentiation, proliferation, migration, and survival [52]. RAS is regulated by the let-7 miRNA family [53] which is among the 20 most expressed miRNAs in Calu-3 and among which 5 miRNAs were significantly downregulated at 24 h. MAPK is also controlled by miR-4728 [54] which was among the 3 most upregulated miRNAs at 24 h and 72 h. Additionally, the most upregulated miRNAs such as miR-1246 and miR-1290 have been reported to be potentially involved in fundamental cellular processes [55,56].

Among other pathways targeted by the upregulated miRNAs, we found cell endocytosis [57] and cholinergic pathways [58] which are of fundamental relevance to the infection process. In the same vein, other downregulated miRNAs are also associated with genes involved in the core of cell survival mechanisms. These include AMPK and PI3K/AKT signalling pathways which are key energy regulators in the cell and participate in host immune function [59,60]. Strategies of the virus versus the host are not so easily distinguished in the modulation of miRNAs; indeed, the overall regulation is likely a combination of co-evolving virus-host strategies. Besides sharing common targets and interacting with each other [61], each miRNA can have an extended

 doi:10.20944/preprints202208.0340.v1

influence on the regulation of mRNAs and their evolution (especially on their 3'UTRs) [12]. This may explain the lack of specificity of GO and KEGG analyses of miRNA target genes.

In this study we explored and confirmed the interactions between upregulated miR-1246 and ACE2 mRNA in Calu-3 cells. Previous study on pulmonary microvascular endothelial cells (PMVECs) reported miR-1246 to repress ACE2 expression by binding to the 3'UTR [62]. By targeting ACE2, miR-1246 mediates pulmonary endothelial cell apoptosis, acute lung injury and acute respiratory distress syndrome (ARDS) [62]. Furthermore, patients with chronic obstructive pulmonary disease or pulmonary hypertension [63–65] demonstrate low miR-1246 expression and high ACE2 expression compared to healthy subjects. Inversely, in relation to ACE2, increased levels of miR-1246 were reported to associate with Acute Respiratory Distress Syndrome (ARDS) [18,62,66]. miR-1246 therefore appears to be a specific and complex biomarker for lung diseases and could be critically informative on the risk of COVID-19 complications.

Given the bioinformatics predictions [66], the experimental validation on two cell types (Calu-3: this study, PMVECs [62]) and the specificity of the interaction, miR-1246 may emerge as a prime "therapeutic" target to modulate ACE2. Although the role of ACE2 is ambiguous in the progression of COVID-19 [67], there is no doubt that its availability remains the major tropism determinant for SARS-CoV-2 [64] and miR-1246 is a game changer in ACE2 provision.

Our qPCR results indicated an upregulation of ACE2 at 24 h and 72 h, but not at 48 h. Same samples, analyzed by RNA-Seq, showed an upregulation of miR-1246 at 24 h and 72 h. This suggests that the repressive effect of miRNA on ACE2 does not occur spontaneously and that it does not necessarily lead to the degradation of the ACE2 mRNA. Indeed, there is current evidence highlighting multiple, non-canonical modes of miRNA-mediated mRNA regulation [68].

We assessed the expression level of numerous transcripts involved in the pathogenesis of SARS-CoV-2. At the transcriptional level, we attempted to explore the correlation between RAS and SARS-CoV-2 which is being extensively studied [69] but still poorly understood. RAS dysregulation observed during SARS-CoV-2 infection is believed to contribute to adverse cardiovascular and respiratory effects, hypercoagulation, and inflammation [70]. First, we found an early and drastic drop in the level of renin which is an upstream player in the RAS enzymatic cascade, suggesting a possible slowdown effect against the viral infection [71]. However, the observed increase of ACE/ACE2 ratio at 24 h seems to be a negative viral effect and is known to be a risk of worse outcomes in COVID-19 infection [72]. At 72 h, the joint augmentation of renin and ACE2 could portend a favorable scenario since both actors direct the protective pathway of RAS system [70]. The accumulation of angiotensinogen, the substrate for the formation of angiotensin I, seemed to be a direct result of renin decrease.

Through its peptidases and interacting receptors, RAS also represents an integrated inflammatory system [73]. We observed an early and transient upregulation of pro-inflammatory biomarkers of signaling pathways which participate in the cellular response triggered by viral infection [74] including CXCL10, whose increased levels usually associate with urgent transfer to the ICU (intensive care unit) or with death [75] and the prime candidate for mediating inflammation in COVID-19, IL-6 [76]. At 72 h, the increase of IFN1β, with its antiviral and immunomodulatory effects [77], seems to overcome the pro-inflammatory actors upregulated at 24 h (CXCL10, IL-6). It should be noted, however, that interferons do not improve outcomes (adverse symptoms and consequences) for hospitalized adults with COVID-19 [78].

However, the above qPCR results only reflect what happens at the transcript level and do not provide information on the expression level of the proteins under these experimental conditions. Further analyses are needed to elucidate the enigmatic role of the enzymes ACE2 and ACE as well as renin in the RAS system in the context of COVID-19.

In conclusion, our study documents new aspects of the pathogenesis of SARS-CoV-2 with the purpose of further reinforcing the available clinical and molecular data. Contradictory results about biological significance of biomarkers, treatments and other clinical parameters related to COVID-19 were observed throughout the pandemic [76].

Conflicts of Interest: The authors declare that the research was conducted in the absence of any commercial or financial relationships that could be construed as a potential conflict of interest.

Author Contributions: Conceptualization, P.P. and K.M.; methodology, I.D., R.A.J., E.V.; writing—original draft preparation, I.D. and E.V.; writing—review and editing, I.D., R.A.J., E.V., R.A.K., K.M. and P.P.; approved submission, all authors. All authors have read and agreed to the published version of the manuscript.

Funding: This research was funded by CIHR (to K.M.) and the CHU de Québec Research Center (to P.P.). The APC was funded by the CHU de Québec Research Center.

Data Availability Statement: The data presented in this study are available on request from the corresponding author.

References

1. COVID-19 Map Available online: https://coronavirus.jhu.edu/map.html (accessed on 17 May 2022).
2. Mousavizadeh, L.; Ghasemi, S. Genotype and Phenotype of COVID-19: Their Roles in Pathogenesis. *J Microbiol Immunol Infect* **2021**, *54*, 159–163, doi:10.1016/j.jmii.2020.03.022.
3. Anand, U.; Jakhmola, S.; Indari, O.; Jha, H.C.; Chen, Z.-S.; Tripathi, V.; Pérez de la Lastra, J.M. Potential Therapeutic Targets and Vaccine Development for SARS-CoV-2/COVID-19 Pandemic Management: A Review on the Recent Update. *Front Immunol* **2021**, *12*, 658519, doi:10.3389/fimmu.2021.658519.
4. Mohamed Khosroshahi, L.; Rokni, M.; Mokhtari, T.; Noorbakhsh, F. Immunology, Immunopathogenesis and Immunotherapeutics of COVID-19; an Overview. *Int Immunopharmacol* **2021**, *93*, 107364, doi:10.1016/j.intimp.2020.107364.
5. Perlman, S.; Netland, J. Coronaviruses Post-SARS: Update on Replication and Pathogenesis. *Nat Rev Microbiol* **2009**, *7*, 439–450, doi:10.1038/nrmicro2147.
6. Hoffmann, M.; Kleine-Weber, H.; Schroeder, S.; Krüger, N.; Herrler, T.; Erichsen, S.; Schiergens, T.S.; Herrler, G.; Wu, N.-H.; Nitsche, A.; et al. SARS-CoV-2 Cell Entry Depends on ACE2 and TMPRSS2 and Is Blocked by a Clinically Proven Protease Inhibitor. *Cell* **2020**, *181*, 271-280.e8, doi:10.1016/j.cell.2020.02.052.
7. Papa, G.; Mallery, D.L.; Albecka, A.; Welch, L.G.; Cattin-Ortolá, J.; Luptak, J.; Paul, D.; McMahon, H.T.; Goodfellow, I.G.; Carter, A.; et al. Furin Cleavage of SARS-CoV-2 Spike Promotes but Is Not Essential for Infection and Cell-Cell Fusion. *PLoS Pathog* **2021**, *17*, e1009246, doi:10.1371/journal.ppat.1009246.
8. Harrison, A.G.; Lin, T.; Wang, P. Mechanisms of SARS-CoV-2 Transmission and Pathogenesis. *Trends Immunol* **2020**, *41*, 1100–1115, doi:10.1016/j.it.2020.10.004.
9. Kim, J.S.; Lee, J.Y.; Yang, J.W.; Lee, K.H.; Effenberger, M.; Szpirt, W.; Kronbichler, A.; Shin, J.I. Immunopathogenesis and Treatment of Cytokine Storm in COVID-19. *Theranostics* **2021**, *11*, 316–329, doi:10.7150/thno.49713.
10. Raman, R.; Patel, K.J.; Ranjan, K. COVID-19: Unmasking Emerging SARS-CoV-2 Variants, Vaccines and Therapeutic Strategies. *Biomolecules* **2021**, *11*, 993, doi:10.3390/biom11070993.
11. Friedman, R.C.; Farh, K.K.-H.; Burge, C.B.; Bartel, D.P. Most Mammalian MRNAs Are Conserved Targets of MicroRNAs. *Genome Res* **2009**, *19*, 92–105, doi:10.1101/gr.082701.108.

12. Bartel, D.P. Metazoan MicroRNAs. *Cell* **2018**, *173*, 20–51, doi:10.1016/j.cell.2018.03.006.
13. El-Nabi, S.H.; Elhiti, M.; El-Sheekh, M. A New Approach for COVID-19 Treatment by Micro-RNA. *Med Hypotheses* **2020**, *143*, 110203, doi:10.1016/j.mehy.2020.110203.
14. Zhang, S.; Amahong, K.; Sun, X.; Lian, X.; Liu, J.; Sun, H.; Lou, Y.; Zhu, F.; Qiu, Y. The MiRNA: A Small but Powerful RNA for COVID-19. *Brief Bioinform* **2021**, *22*, 1137–1149, doi:10.1093/bib/bbab062.
15. Trobaugh, D.W.; Klimstra, W.B. MicroRNA Regulation of RNA Virus Replication and Pathogenesis. *Trends Mol Med* **2017**, *23*, 80–93, doi:10.1016/j.molmed.2016.11.003.
16. Mori, M.A.; Ludwig, R.G.; Garcia-Martin, R.; Brandão, B.B.; Kahn, C.R. Extracellular MiRNAs: From Biomarkers to Mediators of Physiology and Disease. *Cell Metab* **2019**, *30*, 656–673, doi:10.1016/j.cmet.2019.07.011.
17. Condrat, C.E.; Thompson, D.C.; Barbu, M.G.; Bugnar, O.L.; Boboc, A.; Cretoiu, D.; Suciu, N.; Cretoiu, S.M.; Voinea, S.C. MiRNAs as Biomarkers in Disease: Latest Findings Regarding Their Role in Diagnosis and Prognosis. *Cells* **2020**, *9*, E276, doi:10.3390/cells9020276.
18. Marchi, R.; Sugita, B.; Centa, A.; Fonseca, A.S.; Bortoletto, S.; Fiorentin, K.; Ferreira, S.; Cavalli, L.R. The Role of MicroRNAs in Modulating SARS-CoV-2 Infection in Human Cells: A Systematic Review. *Infect Genet Evol* **2021**, *91*, 104832, doi:10.1016/j.meegid.2021.104832.
19. Saulle, I.; Garziano, M.; Fenizia, C.; Cappelletti, G.; Parisi, F.; Clerici, M.; Cetin, I.; Savasi, V.; Biasin, M. MiRNA Profiling in Plasma and Placenta of SARS-CoV-2-Infected Pregnant Women. *Cells* **2021**, *10*, 1788, doi:10.3390/cells10071788.
20. Tang, H.; Gao, Y.; Li, Z.; Miao, Y.; Huang, Z.; Liu, X.; Xie, L.; Li, H.; Wen, W.; Zheng, Y.; et al. The Noncoding and Coding Transcriptional Landscape of the Peripheral Immune Response in Patients with COVID-19. *Clin Transl Med* **2020**, *10*, e200, doi:10.1002/ctm2.200.
21. Li, C.; Hu, X.; Li, L.; Li, J.-H. Differential MicroRNA Expression in the Peripheral Blood from Human Patients with COVID-19. *J Clin Lab Anal* **2020**, *34*, e23590, doi:10.1002/jcla.23590.
22. Wang, S.; Yao, X.; Ma, S.; Ping, Y.; Fan, Y.; Sun, S.; He, Z.; Shi, Y.; Sun, L.; Xiao, S.; et al. A Single-Cell Transcriptomic Landscape of the Lungs of Patients with COVID-19. *Nat Cell Biol* **2021**, *23*, 1314–1328, doi:10.1038/s41556-021-00796-6.
23. Chow, J.T.-S.; Salmena, L. Prediction and Analysis of SARS-CoV-2-Targeting MicroRNA in Human Lung Epithelium. *Genes (Basel)* **2020**, *11*, 1002, doi:10.3390/genes11091002.
24. Wyler, E.; Mösbauer, K.; Franke, V.; Diag, A.; Gottula, L.T.; Arsiè, R.; Klironomos, F.; Koppstein, D.; Hönzke, K.; Ayoub, S.; et al. Transcriptomic Profiling of SARS-CoV-2 Infected Human Cell Lines Identifies HSP90 as Target for COVID-19 Therapy. *iScience* **2021**, *24*, doi:10.1016/j.isci.2021.102151.
25. Banerjee, A.; El-Sayes, N.; Budylowski, P.; Jacob, R.A.; Richard, D.; Maan, H.; Aguiar, J.A.; Demian, W.L.; Baid, K.; D'Agostino, M.R.; et al. Experimental and Natural Evidence of SARS-CoV-2-Infection-Induced Activation of Type I Interferon Responses. *iScience* **2021**, *24*, doi:10.1016/j.isci.2021.102477.
26. Diallo, I.; Ho, J.; Laffont, B.; Laugier, J.; Benmoussa, A.; Lambert, M.; Husseini, Z.; Soule, G.; Kozak, R.; Kobinger, G.P.; et al. Altered MicroRNA Transcriptome in Cultured Human Liver Cells upon Infection with Ebola Virus. *Int J Mol Sci* **2021**, *22*, 3792, doi:10.3390/ijms22073792.
27. Ye, J.; Coulouris, G.; Zaretskaya, I.; Cutcutache, I.; Rozen, S.; Madden, T.L. Primer-BLAST: A Tool to Design Target-Specific Primers for Polymerase Chain Reaction. *BMC Bioinformatics* **2012**, *13*, 134, doi:10.1186/1471-2105-13-134.
28. Livak, K.J.; Schmittgen, T.D. Analysis of Relative Gene Expression Data Using Real-Time Quantitative PCR and the 2(-Delta Delta C(T)) Method. *Methods* **2001**, *25*, 402–408, doi:10.1006/meth.2001.1262.
29. Vester, B.; Wengel, J. LNA (Locked Nucleic Acid): High-Affinity Targeting of Complementary RNA and DNA. *Biochemistry* **2004**, *43*, 13233–13241, doi:10.1021/bi0485732.
30. Diallo, I.; Husseini, Z.; Guellal, S.; Vion, E.; Ho, J.; Kozak, R.A.; Kobinger, G.P.; Provost, P. Ebola Virus Encodes Two MicroRNAs in Huh7-Infected Cells. *International Journal of Molecular Sciences* **2022**, *23*, 5228, doi:10.3390/ijms23095228.
31. McBride, R.; van Zyl, M.; Fielding, B.C. The Coronavirus Nucleocapsid Is a Multifunctional Protein. *Viruses* **2014**, *6*, 2991–3018, doi:10.3390/v6082991.

32. Hoffmann, M.; Kleine-Weber, H.; Pöhlmann, S. A Multibasic Cleavage Site in the Spike Protein of SARS-CoV-2 Is Essential for Infection of Human Lung Cells. *Mol Cell* **2020**, *78*, 779-784.e5, doi:10.1016/j.molcel.2020.04.022.
33. Walls, A.C.; Park, Y.-J.; Tortorici, M.A.; Wall, A.; McGuire, A.T.; Veesler, D. Structure, Function, and Antigenicity of the SARS-CoV-2 Spike Glycoprotein. *Cell* **2020**, *181*, 281-292.e6, doi:10.1016/j.cell.2020.02.058.
34. Coperchini, F.; Chiovato, L.; Croce, L.; Magri, F.; Rotondi, M. The Cytokine Storm in COVID-19: An Overview of the Involvement of the Chemokine/Chemokine-Receptor System. *Cytokine Growth Factor Rev* **2020**, *53*, 25–32, doi:10.1016/j.cytogfr.2020.05.003.
35. Costela-Ruiz, V.J.; Illescas-Montes, R.; Puerta-Puerta, J.M.; Ruiz, C.; Melguizo-Rodríguez, L. SARS-CoV-2 Infection: The Role of Cytokines in COVID-19 Disease. *Cytokine Growth Factor Rev* **2020**, *54*, 62–75, doi:10.1016/j.cytogfr.2020.06.001.
36. Kedzierski, L.; Linossi, E.M.; Kolesnik, T.B.; Day, E.B.; Bird, N.L.; Kile, B.T.; Belz, G.T.; Metcalf, D.; Nicola, N.A.; Kedzierska, K.; et al. Suppressor of Cytokine Signaling 4 (SOCS4) Protects against Severe Cytokine Storm and Enhances Viral Clearance during Influenza Infection. *PLoS Pathog* **2014**, *10*, e1004134, doi:10.1371/journal.ppat.1004134.
37. Kopan, R. Notch Signaling. *Cold Spring Harb Perspect Biol* **2012**, *4*, a011213, doi:10.1101/cshperspect.a011213.
38. Komiya, Y.; Habas, R. Wnt Signal Transduction Pathways. *Organogenesis* **2008**, *4*, 68–75, doi:10.4161/org.4.2.5851.
39. Ji, W.-T.; Liu, H.J. PI3K-Akt Signaling and Viral Infection. *Recent Pat Biotechnol* **2008**, *2*, 218–226, doi:10.2174/187220808786241042.
40. Beyerstedt, S.; Casaro, E.B.; Rangel, É.B. COVID-19: Angiotensin-Converting Enzyme 2 (ACE2) Expression and Tissue Susceptibility to SARS-CoV-2 Infection. *Eur J Clin Microbiol Infect Dis* **2021**, *40*, 905–919, doi:10.1007/s10096-020-04138-6.
41. Ni, W.; Yang, X.; Yang, D.; Bao, J.; Li, R.; Xiao, Y.; Hou, C.; Wang, H.; Liu, J.; Yang, D.; et al. Role of Angiotensin-Converting Enzyme 2 (ACE2) in COVID-19. *Critical Care* **2020**, *24*, 422, doi:10.1186/s13054-020-03120-0.
42. Scialo, F.; Daniele, A.; Amato, F.; Pastore, L.; Matera, M.G.; Cazzola, M.; Castaldo, G.; Bianco, A. ACE2: The Major Cell Entry Receptor for SARS-CoV-2. *Lung* **2020**, *198*, 867–877, doi:10.1007/s00408-020-00408-4.
43. Ouellet, D.L.; Plante, I.; Landry, P.; Barat, C.; Janelle, M.-E.; Flamand, L.; Tremblay, M.J.; Provost, P. Identification of Functional MicroRNAs Released through Asymmetrical Processing of HIV-1 TAR Element. *Nucleic Acids Res* **2008**, *36*, 2353–2365, doi:10.1093/nar/gkn076.
44. Ouellet, D.L.; Vigneault-Edwards, J.; Létourneau, K.; Gobeil, L.-A.; Plante, I.; Burnett, J.C.; Rossi, J.J.; Provost, P. Regulation of Host Gene Expression by HIV-1 TAR MicroRNAs. *Retrovirology* **2013**, *10*, 86, doi:10.1186/1742-4690-10-86.
45. Ouellet, D.L.; Plante, I.; Boissonneault, V.; Ayari, C.; Provost, P. Refractoriness of Hepatitis C Virus Internal Ribosome Entry Site to Processing by Dicer in Vivo. *Journal of Negative Results in BioMedicine* **2009**, *8*, 8, doi:10.1186/1477-5751-8-8.
46. Shin, O.S.; Kumar, M.; Yanagihara, R.; Song, J.-W. Hantaviruses Induce Cell Type- and Viral Species-Specific Host MicroRNA Expression Signatures. *Virology* **2013**, *446*, 217–224, doi:10.1016/j.virol.2013.07.036.
47. Choi, E.-J.; Kim, H.B.; Baek, Y.H.; Kim, E.-H.; Pascua, P.N.Q.; Park, S.-J.; Kwon, H.-I.; Lim, G.-J.; Kim, S.; Kim, Y.-I.; et al. Differential MicroRNA Expression Following Infection with a Mouse-Adapted, Highly Virulent Avian H5N2 Virus. *BMC Microbiol* **2014**, *14*, 252, doi:10.1186/s12866-014-0252-0.
48. Ebert, M.S.; Sharp, P.A. Roles for MicroRNAs in Conferring Robustness to Biological Processes. *Cell* **2012**, *149*, 515–524, doi:10.1016/j.cell.2012.04.005.
49. tenOever, B.R. RNA Viruses and the Host MicroRNA Machinery. *Nat Rev Microbiol* **2013**, *11*, 169–180, doi:10.1038/nrmicro2971.
50. Backes, C.; Meese, E.; Keller, A. Specific MiRNA Disease Biomarkers in Blood, Serum and Plasma: Challenges and Prospects. *Mol Diagn Ther* **2016**, *20*, 509–518, doi:10.1007/s40291-016-0221-4.

51. Kucher, A.N.; Koroleva, Iu.A.; Zarubin, A.A.; Nazarenko, M.S. MicroRNAs as the Potential Regulators of SARS-CoV-2 Infection and Modifiers of the COVID-19 Clinical Features. *Mol Biol* **2022**, *56*, 29–45, doi:10.1134/S0026893322010034.
52. Masliah-Planchon, J.; Garinet, S.; Pasmant, E. RAS-MAPK Pathway Epigenetic Activation in Cancer: MiRNAs in Action. *Oncotarget* **2016**, *7*, 38892–38907, doi:10.18632/oncotarget.6476.
53. Johnson, S.M.; Grosshans, H.; Shingara, J.; Byrom, M.; Jarvis, R.; Cheng, A.; Labourier, E.; Reinert, K.L.; Brown, D.; Slack, F.J. RAS Is Regulated by the Let-7 MicroRNA Family. *Cell* **2005**, *120*, 635–647, doi:10.1016/j.cell.2005.01.014.
54. Liu, Z.; Zhang, J.; Gao, J.; Li, Y. MicroRNA-4728 Mediated Regulation of MAPK Oncogenic Signaling in Papillary Thyroid Carcinoma. *Saudi J Biol Sci* **2018**, *25*, 986–990, doi:10.1016/j.sjbs.2018.05.014.
55. Ghafouri-Fard, S.; Khoshbakht, T.; Hussen, B.M.; Taheri, M.; Samadian, M. A Review on the Role of MiR-1246 in the Pathoetiology of Different Cancers. *Front Mol Biosci* **2021**, *8*, 771835, doi:10.3389/fmolb.2021.771835.
56. Lin, M.; Shi, C.; Lin, X.; Pan, J.; Shen, S.; Xu, Z.; Chen, Q. SMicroRNA-1290 Inhibits Cells Proliferation and Migration by Targeting FOXA1 in Gastric Cancer Cells. *Gene* **2016**, *582*, 137–142, doi:10.1016/j.gene.2016.02.001.
57. Bayati, A.; Kumar, R.; Francis, V.; McPherson, P.S. SARS-CoV-2 Infects Cells after Viral Entry via Clathrin-Mediated Endocytosis. *J Biol Chem* **2021**, *296*, 100306, doi:10.1016/j.jbc.2021.100306.
58. Kopańska, M.; Batoryna, M.; Bartman, P.; Szczygielski, J.; Banaś-Ząbczyk, A. Disorders of the Cholinergic System in COVID-19 Era—A Review of the Latest Research. *Int J Mol Sci* **2022**, *23*, 672, doi:10.3390/ijms23020672.
59. Bhutta, M.S.; Gallo, E.S.; Borenstein, R. Multifaceted Role of AMPK in Viral Infections. *Cells* **2021**, *10*, 1118, doi:10.3390/cells10051118.
60. Khezri, M.R.; Varzandeh, R.; Ghasemnejad-Berenji, M. The Probable Role and Therapeutic Potential of the PI3K/AKT Signaling Pathway in SARS-CoV-2 Induced Coagulopathy. *Cellular & Molecular Biology Letters* **2022**, *27*, 6, doi:10.1186/s11658-022-00308-w.
61. Hill, M.; Tran, N. MiRNA Interplay: Mechanisms and Consequences in Cancer. *Dis Model Mech* **2021**, *14*, dmm047662, doi:10.1242/dmm.047662.
62. Fang, Y.; Gao, F.; Hao, J.; Liu, Z. MicroRNA-1246 Mediates Lipopolysaccharide-Induced Pulmonary Endothelial Cell Apoptosis and Acute Lung Injury by Targeting Angiotensin-Converting Enzyme 2. *Am J Transl Res* **2017**, *9*, 1287–1296.
63. Cazorla-Rivero, S.; Mura-Escorche, G.; Gonzalvo-Hernández, F.; Mayato, D.; Córdoba-Lanús, E.; Casanova, C. Circulating MiR-1246 in the Progression of Chronic Obstructive Pulmonary Disease (COPD) in Patients from the BODE Cohort. *Int J Chron Obstruct Pulmon Dis* **2020**, *15*, 2727–2737, doi:10.2147/COPD.S271864.
64. Zhang, H.; Rostami, M.R.; Leopold, P.L.; Mezey, J.G.; O'Beirne, S.L.; Strulovici-Barel, Y.; Crystal, R.G. Expression of the SARS-CoV-2 ACE2 Receptor in the Human Airway Epithelium. *Am J Respir Crit Care Med* **2020**, *202*, 219–229, doi:10.1164/rccm.202003-0541OC.
65. Wei, C.; Henderson, H.; Spradley, C.; Li, L.; Kim, I.-K.; Kumar, S.; Hong, N.; Arroliga, A.C.; Gupta, S. Circulating MiRNAs as Potential Marker for Pulmonary Hypertension. *PLoS One* **2013**, *8*, e64396, doi:10.1371/journal.pone.0064396.
66. Khan, A.T.-A.; Khalid, Z.; Zahid, H.; Yousaf, M.A.; Shakoori, A.R. A Computational and Bioinformatic Analysis of ACE2: An Elucidation of Its Dual Role in COVID-19 Pathology and Finding Its Associated Partners as Potential Therapeutic Targets. *J Biomol Struct Dyn* 1–17, doi:10.1080/07391102.2020.1833760.
67. Branco, A.C.C.C.; Sato, M.N.; Alberca, R.W. The Possible Dual Role of the ACE2 Receptor in Asthma and Coronavirus (SARS-CoV2) Infection. *Frontiers in Cellular and Infection Microbiology* **2020**, *10*.
68. Nilsen, T.W. Mechanisms of MicroRNA-Mediated Gene Regulation in Animal Cells. *Trends in Genetics* **2007**, *23*, 243–249, doi:10.1016/j.tig.2007.02.011.
69. Vitiello, A.; Ferrara, F. Correlation between Renin-Angiotensin System and Severe Acute Respiratory Syndrome Coronavirus 2 Infection: What Do We Know? *European Journal of Pharmacology* **2020**, *883*, 173373, doi:10.1016/j.ejphar.2020.173373.

70. Wiese, O.J.; Allwood, B.W.; Zemlin, A.E. COVID-19 and the Renin-Angiotensin System (RAS): A Spark That Sets the Forest Alight? *Med Hypotheses* **2020**, *144*, 110231, doi:10.1016/j.mehy.2020.110231.
71. Bavishi, C.; Maddox, T.M.; Messerli, F.H. Coronavirus Disease 2019 (COVID-19) Infection and Renin Angiotensin System Blockers. *JAMA Cardiology* **2020**, *5*, 745–747, doi:10.1001/jamacardio.2020.1282.
72. Pagliaro, P.; Penna, C. ACE/ACE2 Ratio: A Key Also in 2019 Coronavirus Disease (Covid-19)? *Frontiers in Medicine* **2020**, *7*.
73. Bastolla, U.; Chambers, P.; Abia, D.; Garcia-Bermejo, M.-L.; Fresno, M. Is Covid-19 Severity Associated With ACE2 Degradation? *Frontiers in Drug Discovery* **2022**, *1*.
74. Barbu, M.G.; Condrat, C.E.; Thompson, D.C.; Bugnar, O.L.; Cretoiu, D.; Toader, O.D.; Suciu, N.; Voinea, S.C. MicroRNA Involvement in Signaling Pathways During Viral Infection. *Front Cell Dev Biol* **2020**, *8*, 143, doi:10.3389/fcell.2020.00143.
75. Lorè, N.I.; De Lorenzo, R.; Rancoita, P.M.V.; Cugnata, F.; Agresti, A.; Benedetti, F.; Bianchi, M.E.; Bonini, C.; Capobianco, A.; Conte, C.; et al. CXCL10 Levels at Hospital Admission Predict COVID-19 Outcome: Hierarchical Assessment of 53 Putative Inflammatory Biomarkers in an Observational Study. *Molecular Medicine* **2021**, *27*, 129, doi:10.1186/s10020-021-00390-4.
76. Rubin, E.J.; Longo, D.L.; Baden, L.R. Interleukin-6 Receptor Inhibition in Covid-19 — Cooling the Inflammatory Soup. *New England Journal of Medicine* **2021**, *384*, 1564–1565, doi:10.1056/NEJMe2103108.
77. Samuel, C.E. Antiviral Actions of Interferons. *Clin Microbiol Rev* **2001**, *14*, 778–809, table of contents, doi:10.1128/CMR.14.4.778-809.2001.
78. Kalil, A.C.; Mehta, A.K.; Patterson, T.F.; Erdmann, N.; Gomez, C.A.; Jain, M.K.; Wolfe, C.R.; Ruiz-Palacios, G.M.; Kline, S.; Pineda, J.R.; et al. Efficacy of Interferon Beta-1a plus Remdesivir Compared with Remdesivir Alone in Hospitalised Adults with COVID-19: A Double-Blind, Randomised, Placebo-Controlled, Phase 3 Trial. *The Lancet Respiratory Medicine* **2021**, *9*, 1365–1376, doi:10.1016/S2213-2600(21)00384-2.